ACS APPLIED MATERIALS & INTERFACES

Research Article

www.acsami.org

In Situ Assembly in Confined Spaces of Coated Particle Scaffolds as Thermal Underfills with Extraordinary Thermal Conductivity

Guo Hong,[†] Thomas M. Schutzius,[†] Severin Zimmermann,[†] Brian R. Burg,[‡] Jonas Zürcher,[‡] Thomas Brunschwiler,[‡] Giulia Tagliabue,[†] Bruno Michel,[‡] and Dimos Poulikakos*[,†]

[†]Laboratory of Thermodynamics in Emerging Technologies, Department of Mechanical and Process Engineering, ETH Zurich, Sonneggstrasse 3, 8092 Zurich, Switzerland

[‡]IBM Research−Zurich, Säumerstrasse 4, 8803 Rüschlikon, Switzerland

Supporting Information

ABSTRACT: In situ assembly of high thermal conductivity materials in severely confined spaces is an important problem bringing with it scientific challenges but also significant application relevance. Here we present a simple, affordable, and reproducible methodology for synthesizing such materials, composed of hierarchical diamond micro/nanoparticle scaffolds and an ethylenediamine coating. An important feature of the assembly process is the utilization of ethylenediamine as an immobilizing agent to secure the integrity of the microparticle scaffolds during and after each processing step. After other liquid components employed in the scaffolds assembly dry out, the immobilization agent solidifies forming a stable coated particle scaffold structure. Nanoparticles tend to concentrate in the shell and neck regions between adjacent microparticles. The interface between core and shell, along with the concentrated neck regions of nanoparticles, significantly enhance the thermal conductivity, making such materials an excellent candidate as thermal underfills in the electronics industry, where efficient heat removal is a major stumbling block toward increasing packing density. We show that the presented structures exhibit nearly 1 order of magnitude improvement in thermal conductivity, enhanced temperature uniformity, and reduced processing time compared to commercially available products for electronics cooling, which underpins their potential utility.

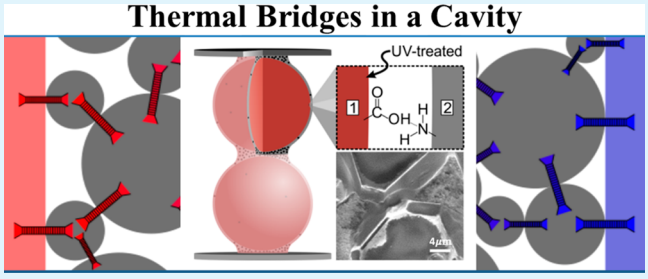

KEYWORDS: *hierarchical composite, liquid bridge, confined space, thermal conductivity, electronics cooling*

1. INTRODUCTION

Materials with advanced thermal properties—often concurrently with other necessary functionalities—are becoming increasingly important as we strive toward achieving an energy-efficient and secure future. Examples for the need of such materials come from the requirements of efficient heat dissipation in many areas, such as complementary metal-oxide semiconductors,[1] light-emitting diodes,[2] and hypersonic re-entry vehicles.[3] A rigid criterion for the development of such materials is often their implementation within an optimized chain of fabrication steps, which necessitates additional concurrent functionalities related to material placement and integrity. With respect to the thermal resistance reduction in multicomponent structures, the heat dissipation material often needs to be filled into a prefabricated severely confined space (e.g., micro cavity), which dramatically affects the morphology and composition of employed materials, without relaxing the key requirement of outstanding heat-transfer performance. This situation becomes even more demanding for multilayer electronic systems (Figure 1a), where the heat must travel a much longer path, and the heat-dissipating thermal underfill layers are organized in complex geometries. The need for significant improvements in the state of the art of such materials is clear.

In general, two approaches are utilized to achieve this goal: (1) microparticle plus epoxy backfilling (e.g., aluminum oxide,[4] boron nitride,[5] and diamond[6,7]); (2) nanoparticle-laden epoxy (e.g., carbon nanotubes[8] and graphene flakes[9,10]). In these approaches, the choice of the candidate particles is based on their excellent bulk thermal conductivities (e.g., 3300 W m^{-1} K^{-1} for diamond[11] and 1300−5300 W m^{-1} K^{-1} for graphene flakes[12−15]), but the reported performances show a 3 orders of magnitude drop due to the nonpercolated structure (Figure 1b),[16,17] which is dominated by the contact resistance at the particle-epoxy interface and the poor thermal conductivity inherent to epoxy (heat channeling resistance, Supporting Information, Figure S1a,b).[18] To exemplify, consider the thermal conductivity of the current commercial thermal underfill based on silicon dioxide (k = 0.4 W m^{-1} K^{-1})[19] with bulk epoxy (k = 0.2 W m^{-1} K^{-1}). Several inherent limitations of epoxy-based particle composites for confined

Received: October 22, 2014
Accepted: December 8, 2014
Published: December 8, 2014

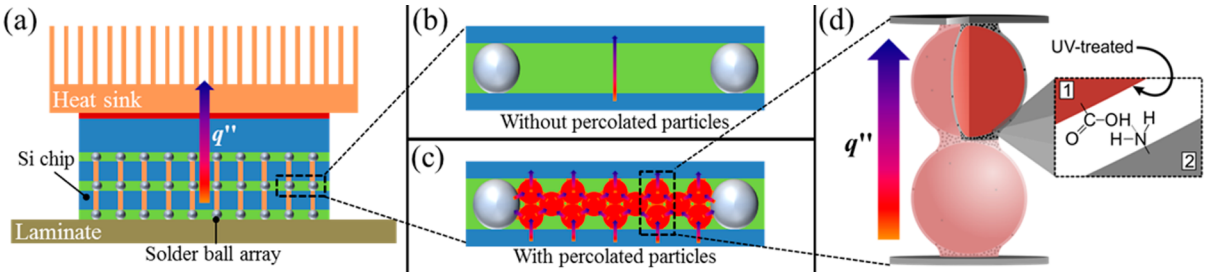

Figure 1. (a) Schematic of the multilayer electronic system. Each layer of the silicon chips is connected/separated by solder ball arrays. (b) Nonpercolated thermal underfill material (low heat dissipation) filled in the microcavity between silicon chips. (c) Percolated thermal underfill material (high heat dissipation) filled in the microcavity between silicon chips. (d) Schematic of the proposed core–shell structure consisting of diamond micro/nanoparticle composites with ethylenediamine coating. (inset, c) The thermal interface resistance is reduced by the interaction between the –COOH terminals from UV-treated diamond surface (**1**) and the $-NH_2$ terminals from ethylenediamine (**2**).

spaces are addressed next. (1) Underfill composite materials based upon epoxy usually have a poor distribution of micro/nanoparticles within the epoxy phase. Such nonuniformities significantly contribute to the generation of hot spots in devices (Supporting Information, Figure S1c,d). (2) Epoxy itself does not favor the filler particle surfaces, which leads to high thermal contact resistance. (3) It has relatively high viscosity, which makes processing time in microcavities prohibitively long (even worse for porous structures). (4) It has a predefined maximum filling time in the cavity, since it simultaneously undergoes cross-linking (i.e., solidification). What is needed is a percolated thermal highway (Figure 1c) and a shift from the epoxy-particle paradigm.

Here we present a systematic approach leading to the synthesis of high performance, thermal transport materials circumventing the aforesaid problems, by generating scaffolds of core–shell structures composed of micro/nanoparticles and an immobilizing/interfacial agent coating (Figure 1d). To fabricate these structures in situ under confinement, we develop a multistep process so as to minimize the destructive capacity of any given process force (e.g., surface tension) acting in these cavities during the assembly of the composite material. The main feature of this assembly process is the utilization of an immobilizing agent to secure the integrity of the delicate microparticle scaffolds during and after each processing step. What makes this immobilizing agent unique is that it also serves as an interfacial agent that interacts strongly with the microparticles and substantially reduces the interfacial thermal resistance. It also has a much lower viscosity during processing (in contrast with epoxy), but solidifies after, which confers mechanical stability. Concentrated regions of nanoparticles occupy the shells and in particular the neck regions between adjacent microparticle core structures. The well-formed interface between core and shell, along with the concentrated neck regions of nanoparticles, result in significantly enhanced thermal conductivity behavior. Although the approach can work with a broad palette of combinations of high thermal conductivity micro- and nanoparticles, a synthetic diamond micro/nanocomposite is considered to be one of the best candidates. This is because of the good performance/price ratio of these particles, and the fact that they satisfy additional requirements in many high-frequency electronic systems, like electrical insulation and low dielectric constant.

2. EXPERIMENTAL SECTION

2.1. Particle Scaffold Assembly. The diamond microparticles were first treated with ultraviolet (UV) irradiation and then filled into the cavities via centrifugation. The immobilization agent (ethylenediamine) was applied by a prewetting method, which will be fully described in the Results and Discussion section. After drying out of the carrier liquid, the diamond nanosuspension was imbibed into the cavity. The immobilization agent underwent a dissolution-reconstruction process and forming a coating with the diamond nanoparticles in the shell and neck regions between adjacent microparticles, as will be fully described in the Results and Discussion section.

2.2. Model Cavities. Two kinds of cavities (glass–silicon and silicon–silicon) were fabricated to study the geometry/composition and thermal performance of the particle scaffolds, respectively. The cavities were made by reactive ion etching of silicon, with a height of 60 μm (typical height between the silicon chip and laminate in electronic systems). A glass cover was attached by anodic bonding and a silicon cover was attached by polyimide thermal-compression bonding, respectively, according to the desired cavity outcome.

2.3. Microparticles. Synthetic diamond microparticles (20–30 μm in diameter) were used as the microscale, thermal conductive filler. Spherical silica particles (53 μm in diameter) were used to illustrate the filling process. All particles were provided by Reishauer AG, Switzerland.

2.4. Nanosuspension. The diamond nanosuspension was provided by Buhler AG, Germany. For all the cases discussed below, a diamond nanoparticle suspension (0.5 vol % in deionized water) was used.

2.5. UV Irradiation. The UV source employed is an ELC-4001 UV light system (Electro-lite corporation), with an output of 13.3 mW cm^{-2}. The irradiation lasted for 4 h, and the container was shaken every 30 min to maintain a uniform irradiation for each particle.

2.6. Microparticle Centrifugation. The introduction of diamond microparticles into the cavities was performed in a homemade centrifugation machine modified from a spin-coater. The spin speed is 150 r min^{-1}. By changing the spin direction repeatedly, cavities can be fully filled.

2.7. Vacancy Ratio Calculation. For all the optical images of the particle bed, the vacancy ratio was calculated via color contrast using the software ImageJ. When particles are displaced by fluid imbibition, the vacancy areas will appear a different color contract from the particle bed areas. The vacancy ratio is calculated as the vacancy portion of the entire area.

2.8. Thermal Measurement. Thermal measurements were performed in a homemade buck sample tester (Supporting Information, Figure S2). The samples were placed between two copper pillars equipped with resistive heaters and six thermocouples on each pillar. Liquid metal (GaIn) is used to reduce the contact resistance between copper pillar and sample. Each sample was measured three times, and the reported data was on average.

3. RESULTS AND DISCUSSION

In general, the thermal conductivity of a composite can be improved by varying the concentration of the high thermally conductive materials in the given space.[20] For nonmetallic

materials, microparticles are the preferred choice since their thermal behavior is governed by phonon transport, and they are not prone to phonon scattering in the way that their nanoparticle counterparts are. However, adjacent microparticles are susceptible to large contact resistances (e.g., point contacts), which is something that the interfacial agent employed here—which forms a shell around microparticles and connecting neck structures in between—can reduce. To reduce the heat channeling resistance of such an interfacial agent—due to its relatively low bulk thermal conductivity—we introduce thermally conductive nanoparticles into the neck region. Thus, the synergistic combination of microparticles, nanoparticles, and interfacial agent results in a hierarchical core−shell structure, promising to drastically improve the heat transfer performance, and forms the basis for the proposed material design.

Let us briefly consider the design and construction of the hierarchical particle scaffolds and their main advantages over the stochastic epoxy-particle composites. Once the microparticles are filled into the cavity (in this work through centrifugation),[21] the initially simple empty space becomes a porous structure ready for the insertion of the immobilizing/interfacial agent and the nanoparticles. In the case of the nanoparticles, there are two possibilities: (1) uniformly dispersed in the pores created by the microparticles, for example, filled via nanoparticle laden polymer (stochastic); (2) condensed as capillary bridges between microparticles, for example, filled via nanosuspension (bridge, Supporting Information, Figure S3a). To assess the effectiveness of a stochastic structure as compared with a bridge structure, the effective thermal conductivity between two microparticles is calculated as a function of nanoparticle bridge radius and nanoparticle concentration. For practical conditions, the stochastic structure is much less efficient at creating high-density (percolating) nanoparticle regions as compared with the bridge structure (Figure S3b); therefore, the bridge structure is a much more efficient thermal structure than the stochastic structure (Figure S3c; see Supporting Information for derivation). This is important because in reality, filling all of the void space in a microparticle bed with nanoparticles is impractical. In addition, the amount of nanoparticles which can be delivered is limited by the rising viscosity of the nanoparticle suspension, which increases with particle concentration in the carrier liquid; increased viscosity makes filling much more difficult when considering flow in porous structures.[6] As a result, the point is not to have a large quantity of poor quality thermal conductors but a smaller quantity of high-quality thermal ones.

Next we consider the processing issues associated with materials designed to occupy prefabricated narrow cavities, specifically for pre-existing microparticle beds. Wet processing is the preferred technique since liquids, if wettable to the porous matrix, can move freely via capillary forces (pumpless transport).[22] Other techniques, such as vapor processing, suffer from nonuniform pressure gradients through the winding structures. Those same winding structures (no clear path) restrict the use of solid processing techniques too. The largest drawback of wet-processing is that it may displace the microparticle bed and result in undesirable hot spots. Three important forces are involved in this situation (Figure 2a), namely, surface tension (F_σ), inertia (F_i), and interparticle (F_j). Because of the small scales of flows in our system, the strongest force is the surface tension (see Supporting Information for a comparison of the importance of the relevant forces capable of disrupting the microparticle bed).

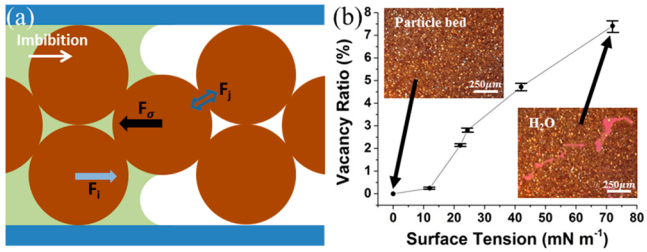

Figure 2. (a) Schematic of the relevant forces involved in the wet-processing techniques within the microparticle bed. (1) Surface tension (F_σ) of a fluid interface on a particle; (2) Inertia (F_i), where the motion of the fluid impinges on an immersed particle (drag, skin drag, etc.). (3) Interparticle (F_j) of the neighboring particles. As the concentration of the particles increases, they tend toward a *jammed* state, resisting all imposed forces and contributing to matrix integrity. (b) Plot of displacements of the microparticle bed caused by fluids with different surface tension. Five liquids of different surface tension (σ_{lv}), i.e., tetradecafluorohexane (C_6F_{14}, σ_{lv} = 12 mN m^{-1}), ethanol (σ_{lv} = 22 mN m^{-1}), 20 vol % ethylenediamine in ethanol (24.4 mN m^{-1}, measured by pendant drop method), ethylenediamine (42 mN m^{-1}), and deionized water (σ_{lv} = 72 mN m^{-1}) were used to analyze the movement behavior. The top left inset is the top view of the particle bed, and the bottom right inset is the result after imbibing water.

To observe the effect of surface tension (of the imbibing fluid) on particle movement, a glass−silicon cavity (Supporting Information, Figure S4) was made to simulate a confined space and was filled with diamond microparticles through centrifugation.[21] The top left inset in Figure 2b is the top view of the microparticle bed through the glass cover. Five liquids with varying surface tension values (σ_{lv} =12−72 mN m^{-1}) were used to analyze the movement behavior. To quantify the displacement of microparticles as a result of liquid imbibition, we define a parameter: the vacancy ratio, ϕ. It is the portion of the cavity area devoid of microparticles compared to the entire particle bed area ($\phi = A_{void}/A_{total}$). From Figure 2b, it is clear that ϕ correlates strongly with σ_{lv} and that there is a threshold of σ_{lv} below which ϕ is negligibly small (~10 mN m^{-1}, i.e., fluorocarbon liquids). Therefore, the surface tension of the carrier liquids should always be minimized when filling the microparticle bed to avoid particle displacement. Since the interfacial agent and the nanoparticle suspension may have high surface tension values (e.g., water-based suspensions), a different processing strategy must be developed.

To reduce the movement of microparticles while imbibing the nanoparticle suspension (filling into the cavity),[23] the microparticles should be immobilized as well as possible. One simple way is to create a liquid bridge between the microparticles, which is an approach intuitively used in the construction of sand castles.[24,25] Ethylenediamine (EN) was chosen as the immobilizing agent, due to its low-volatility (vapor pressure 1.3 kPa at 20 °C), intermediate value of surface tension (42 mN m^{-1}), high solubility in most solvents (e.g., ethanol, water), and tendency to solidify with long-term exposure to air/water vapor.

Before they were introduced into the cavity, diamond microparticles were pretreated by UV irradiation to functionalize their surfaces with −COOH terminals, which have electrostatic interactions with the $-NH_2$ terminals of EN, aiming at the reduction of interfacial resistance (Figure 1c).[26,27] For better observation, spherical silica particles were used to

dx.doi.org/10.1021/am5073222 | ACS Appl. Mater. Interfaces 2015, 7, 838−844

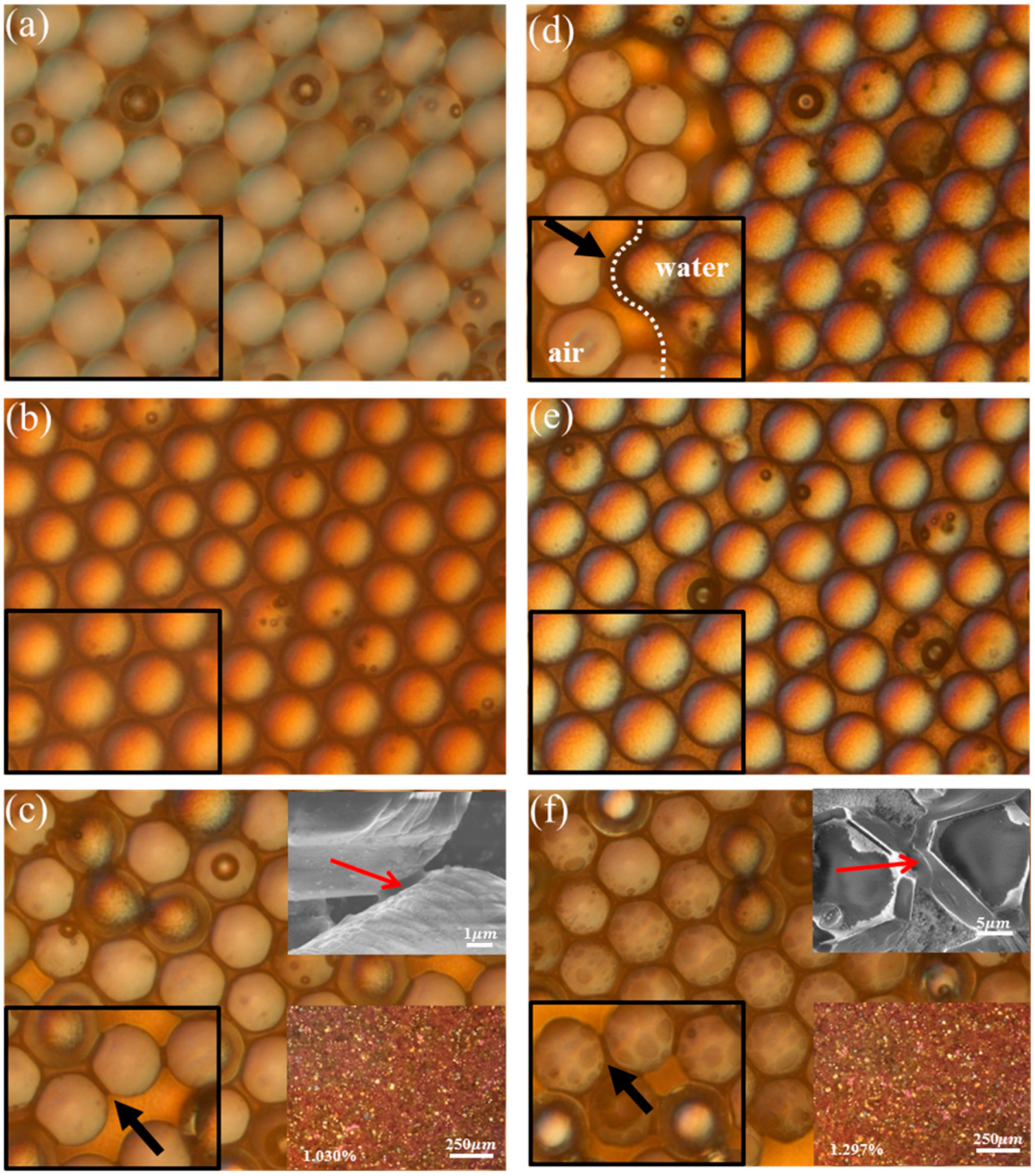

Figure 3. Optical images showing the microparticle bed after each processing step in the construction of particle scaffolds. Instead of 20−30 μm diamond microparticles, 53 μm silica spheres were used here as a model for clearer observation of the phenomena of interest. In all the images, black frames show magnified areas of the particle bed; black arrows indicate the existence of EN bridges between model silica particles; red arrows indicate the existence of EN bridges between diamond particles in the real underfill matrix. (a) Silica microparticle bed. (b) Silica particle bed wetted by ethylenediamine/ethanol mixture. (c) Ethylenediamine liquid bridges between silica microparticles. (inset, upper right) The corresponding SEM image of the EN liquid bridge between two diamond particles. (inset, lower right) The optical image of the diamond particle bed of the real underfill material. (d) Interface between dry and wet particles as the water-based nanoparticle suspension is introduced. The ethylenediamine liquid bridge still exists in the dry bed and disappears (dissolves) in the wetted bed. (e) EN bridges dissolve completely when the nanosuspension wets the entire particle bed. (f) Ethylenediamine liquid bridges reconstructed between silica microparticles. (inset, upper right) The corresponding SEM image of the diamond particles. (inset, lower right) The optical image of the diamond particle bed (real thermal underfill). A uniform coating is found for diamond particles due to the UV functionalization. The coating on the silica particles consists of random spots.

illustrate the filling process. Figure 3a is the assembled silica particle bed via centrifugation. Considering its relatively large value of σ_{lv}, EN cannot be directly introduced into the cavity; otherwise, it will result in a relatively large vacancy (ϕ = 4.7%, Figure 2b). So instead of allowing surface tension to drive the filling process of EN, we preimbibe the cavity with an immiscible, volatile, low surface-tension liquid (C_6F_{14}), which by virtue of evaporation will create a natural pressure gradient in the cavity drawing the EN (20 vol % in ethanol) inward. By utilizing an immiscible preimbibing fluid, the interfacial tension experienced by the particles at the two-fluid interface is expected to be substantially reduced as compared with EN and air (more details on the filling process are illustrated in Supporting Information, Figure S5). Figure 3b shows an image of the silica particle after the EN solution was introduced through the aforesaid process—note that minimal displacement of the particles occurred.

Figure 3c shows images of EN liquid bridges between silica particles formed by capillary forces after the carrier solvent (ethanol) for EN has dried out. The upper-right inset image is

dx.doi.org/10.1021/am5073222 | ACS Appl. Mater. Interfaces 2015, 7, 838−844

the corresponding SEM image of the EN liquid bridge between two diamond particles; the lower-right inset is the optical image of the diamond particle bed after the same processing steps. Even though care was taken to reduce the effect of surface tension during EN filling, ϕ increases from 0.25% to ~1%; however, this result is greatly improved compared to the case of free imbibition of EN/ethanol mixture (ϕ = 2.8%, Figure 2b). The so-formed EN liquid bridges between adjacent microparticles enhance mechanical stability and enable the subsequent imbibition of the diamond nanoparticle suspension. To insert nanoparticles into the neck regions, such EN liquid bridges are designed with a temporary nature; they will dissolve into water after the fluid interface crosses over them (Figure 3d), after which point no destabilizing interfacial tension is applied on the microparticles. This filling process is rapid (5 mm/s) and is capable of covering large dimensions in confined spaces (Figure 3e). After the evaporation of water at the end of the filling process, all the remaining materials (EN and nanoparticles, Supporting Information, Figure S6) are transported by capillarity into the confined neck space between microparticles, without causing serious displacement (Figure 3f). In Figure 3f, the top right and bottom right inset images are the corresponding SEM and optical images of the diamond particles after all processing steps, respectively. The vacancy ratio after all processing steps is ϕ = 1.3%, a significant improvement compared to water-based processing techniques alone (ϕ = 7.4%, Figure 2b). Over time, after EN is exposed to water/air, it eventually solidified (Supporting Information, Figure S7). Since the diamond microparticles were treated with UV, a uniform coating of EN on diamond surfaces is observed compared to the random dots on silica surface. This is because of the electrostatic interaction between −COOH terminals of the functionalized diamond and $-NH_2$ terminals of EN. Such uniform coating may also contribute significantly toward maintaining the mechanical integrity of the scaffolds (these structures can survive under nitrogen flow of ~100 m s^{-1}).

Now that uniform thermal channels have been fabricated, their actual thermal performance is investigated. A silicon−silicon cavity was fabricated to measure the thermal conductivity and the uniformity of the diamond composites. In the case of a packed bed of diamond microparticles, the effective thermal resistance was found to be quite high (No. 2 in Figure 4). The UV treatment of diamond microparticles plays an important role to improve the contact between microparticles and EN. There is a 4-fold drop in thermal resistance with UV treatment (comparing Nos. 3 and 4 in Figure 4). We attribute this to the electrostatic interaction between the −COOH terminals on functionalized diamond surface and the $-NH_2$ groups on EN, which reduces the interfacial resistance. After imbibing the nanosuspension, the thermal resistance further decreases due to the generation of a thermally conductive structure of nanoparticles within the necks. In addition, as discussed above, the shells and necks solidify after this last step, providing a long-term sustainable scaffold with excellent thermal conductivity performance, without deterioration issues due to EN bridge evaporation with time. This topic is discussed in detail in the following.

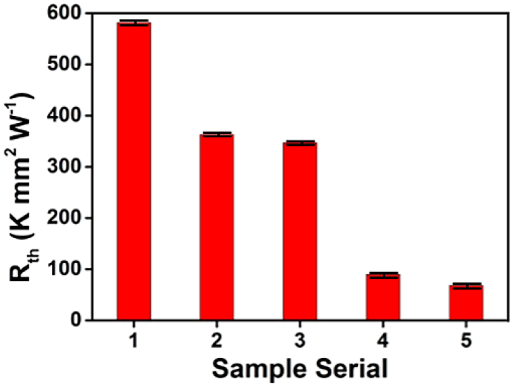

Figure 4. Effective thermal resistance of different filling stages: (1) Empty cavity; (2) diamond microparticle bed; (3) untreated diamond microparticle with ethylenediamine liquid bridges; (4) UV-treated diamond microparticle with ethylenediamine liquid bridges; (5) diamond micro/nanoparticle composite with ethylenediamine coating.

With all real-world applications, after the issue of performance has been addressed, the issue of stability arises. Because of its inherent low volatility, the EN liquid bridge (before imbibing the nanosuspension) was expected to evaporate slowly over time. As shown by the black line in Figure 5a, the thermal resistance of microparticles with EN liquid bridge almost doubled after two weeks. However, after imbibing the nanosuspension, the thermal resistance decreases over time and finally becomes stable (red line in Figure 5a). We speculate that the coupling between EN and water reduces the evaporation rate of the liquid bridge and at the end a solid material is generated (Supporting Information, Figure S7).

Uniformity of the composites is also essential to avoid hot spots in thermal underfill materials. Figure 5b is the temperature map from an infrared camera with a resolution of 100 μm. The heat dissipation is shown to be uniform, due to the absence of sizable vacancies resulting from the force competition during the filling process. As a result, the two walls of the cavity are connected by a large network of heat pathways, which are composed by 2−3 microparticles and the corresponding nanoparticle necks (considering the diameter of the filling particles and the height of the cavity, no more than three particles can be arranged in the direction of the heat flux). As mentioned in the beginning, in addition to the obvious difficulty in its insertion in a confined space, the current commercial underfill based on silicon dioxide has a thermal conductivity of only k = 0.4 W m^{-1} K^{-1} (No. 1 in Figure 5c).[19] Our diamond composite, in situ assembled under confinement, improves this by nearly an order of magnitude to k = 3.1 W m^{-1} K^{-1} (No. 4 in Figure 5c).

4. CONCLUSIONS

A novel systematic methodology for in situ synthesis of high-performance thermal underfill materials in confined spaces common in the electronics industry was presented. The thermal channels in the material, significantly enhancing the heat-transfer performance, are realized with core−shell structures composed of hierarchical diamond micro/nanoparticle scaffolds, coated with ethylenediamine. This approach advances the state of the art beyond epoxy-based techniques, which are typically used to form thermally conductive layers in electronics cooling. We demonstrated that such (mechanically stable) structures exhibit greatly improved thermal conductivity (nearly 1 order of magnitude improvement compared to commercial products), temperature uniformity, thermal stability, and processing time. The construction of thermal channels in this study was demonstrated based upon diamond particles, but the method is applicable to a variety of other materials in particle

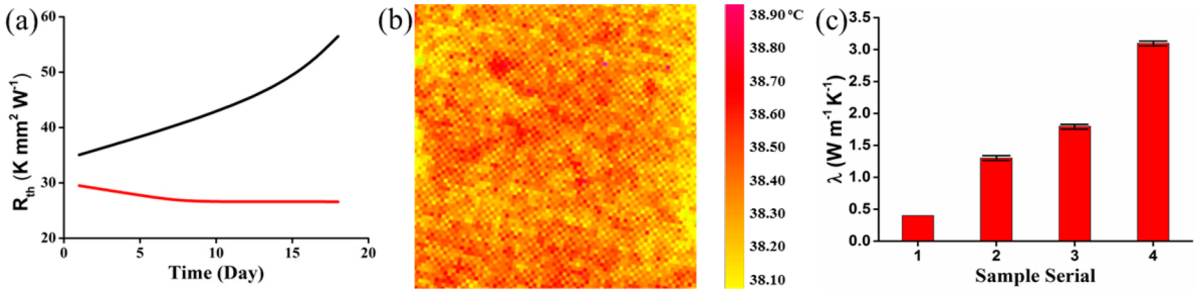

Figure 5. Thermal properties of diamond microparticle composites. (a) Time dependence of the effective thermal resistance of immobilized diamond microparticles with (red line) and without (black line) diamond nanoparticles. (b) Optical image of the cavity captured from high-resolution IR camera. The total area is 7 cm × 7 cm and each pixel represents an area of 100 × 100 μm^2. (c) Thermal conductivity of different underfills: (1) Commercial underfill based on silicon dioxide;[21] (2) diamond microparticle with epoxy backfilling; (3) diamond microparticle with ethylenediamine liquid bridges; (4) diamond micro/nanoparticle composite with ethylenediamine coating.

form and is also valuable for other heat-transfer applications in confined spaces.

■ ASSOCIATED CONTENT

Ⓢ Supporting Information

Analysis of the effective thermal conductivity of the hierarchical particle scaffolds, analysis of forces acting on the microparticle bed during construction of the hierarchical particle scaffolds, optical image of cavities, schematic of the filling process, SEM image of nanoparticle bridges, optical image of the bulk thermal tester, optical image of ethylenediamine−water mixture after solidification. This material is available free of charge via the Internet at http://pubs.acs.org.

■ AUTHOR INFORMATION

Corresponding Author

*E-mail: dpoulikakos@ethz.ch.

Notes

The authors declare no competing financial interest.

■ ACKNOWLEDGMENTS

Financial support for this project is provided by the Commission of Technological Innovation (CTI), Switzerland, under the Project HiPerCon (No. 1473.4). T.M.S. gratefully acknowledges the ETH Zurich Postdoctoral Fellowship Program and Marie Curie Actions for People COFUND program (FEL-14 13-1). We thank U. Drechsler from IBM Research−Zurich for fabricating the glass−silicon and silicon−silicon cavities, M. Dvorak and S. Guenther from Reishauer AG for the supply of diamond microparticles, K. Gossmann and K. Steingroever from Buhler for the supply of diamond nanosuspension and for their valuable input to this project.

■ REFERENCES

(1) Lin, S. C.; Banerjee, K. Cool Chips: Opportunities and Implications for Power and Thermal Management. *IEEE Trans. Electron Devices* **2008**, *55*, 245−255.

(2) Arik, M.; Weaver, S. Chip Scale Thermal Management of High Brightness LED Packages. *Proc. SPIE* **2004**, *5530*, 214−223.

(3) Monteverde, F.; Scatteia, L. Resistance to Thermal Shock and to Oxidation of Metal Diborides− SiC Ceramics for Aerospace Application. *J. Am. Ceram. Soc.* **2007**, *90*, 1130−1138.

(4) Brunschwiler, T.; Goicochea, J.; Matsumoto, K.; Wolf, H.; Kümin, C.; Michel, B.; Wunderle, B.; Faust, W. In *Formulation of Percolating Thermal Underfill by Sequential Convective Gap Filling*, Proceedings of 7th International Conference and Exhibition on Device Packaging, Scottsdale, AZ, Mar 8−11; IMAPS: Washington, DC, 2011, Vol. *4*, pp 229−237.

(5) Liang, Q.; Moon, K. S.; Wong, C. P. In *High Thermal Conductive Underfill Materials for Flip-Chip Application*, Proceedings of 2nd IEEE International Interdisciplinary Conference on Portable Information Devices 2008 and the 7th IEEE Conference on Polymers and Adhesives in Microelectronics and Photonics 2008, Garmisch-Partenkirchen, Germany, Aug 17−20; IEEE: New York, 2008, pp 162−165.

(6) Lee, W. S.; Han, I. Y.; Yu, J.; Kim, S. J.; Byun, K. Y. In *Thermal Characterization of Thermally Conductive Underfill for a Flip-chip Package using Novel Temperature Sensing Technique*, Proceedings of 6th Electronics Packaging Technology Conference 2004, Singapore, Dec 8−10; IEEE: New York, 2004, pp 47−52.

(7) Lee, W. S.; Yu, J. Diam. Comparative Study of Thermally Conductive Fillers in Underfill for the Electronic Components. *Diamond Relat. Mater.* **2005**, *14*, 1647−1653.

(8) Biercuk, M. J.; Llaguno, M. C.; Radosavljevic, M.; Hyun, J. K.; Johnson, A. T.; Fischer, J. E. Carbon Nanotube Composites for Thermal Management. *Appl. Phys. Lett.* **2002**, *80*, 2767.

(9) Veca, L. M.; Meziani, M. J.; Wang, W.; Wang, X.; Lu, F.; Zhang, P.; Lin, Y.; Fee, R.; Connell, J. W.; Sun, Y. P. Carbon Nanosheets for Polymeric Nanocomposites with High Thermal Conductivity. *Adv. Mater.* **2009**, *21*, 2088−2092.

(10) Shahil, K. M. F.; Balandin, A. A. Graphene−Multilayer Graphene Nanocomposites as Highly Efficient Thermal Interface Materials. *Nano Lett.* **2012**, *12*, 861−867.

(11) Wei, L.; Kuo, P. K.; Thomas, R. L. Thermal Conductivity of Isotopically Modified Single Crystal Diamond. *Phys. Rev. Lett.* **1993**, *70*, 3764−3767.

(12) Ghosh, S.; Bao, W.; Nika, D. L.; Subrina, S.; Pokatilov, E. P.; Lau, C. N.; Balandin, A. A. Dimensional Crossover of Thermal Transport in Few-layer Graphene. *Nat. Mater.* **2010**, *9*, 555−558.

(13) Balandin, A. A. Thermal Properties of Graphene and Nanostructured Carbon Materials. *Nat. Mater.* **2011**, *10*, 569−581.

(14) Balandin, A. A.; Ghosh, S.; Bao, W.; Calizo, I.; Teweldebrhan, D.; Miao, F.; Lau, C. N. Superior Thermal Conductivity of single layer graphene. *Nano Lett.* **2008**, *8*, 902−907.

(15) Xu, X.; Pereira, L. F. C.; Wang, Y.; Wu, J.; Zhang, K.; Zhao, X.; Bae, S.; Bui, C. T.; Xie, R.; Thong, J. T. L.; Hong, B. H.; Loh, K. P.; Donadio, D.; Li, B.; Özyilmaz, B. Length-dependent Thermal Conductivity in Suspended Single-layer Graphene. *Nat. Commun.* **2014**, *5*, 3689.

(16) Goicochea, J. V; Brunschwiler, T.; Zürcher, J.; Wolf, H.; Matsumoto, K.; Michel, B. In *Enhanced Centrifugal Percolating Thermal Underfills based on Neck Formation by Capillary Bridge*, Proceedings of 13th IEEE Intersociety Conference on Thermal and Thermomechanical Phenomena in Electronic Systems, San Diego, CA, May 30−June 1; IEEE: New York2012, pp 1234−1241.

(17) Song, S. H.; Park, K. H.; Kim, B. H.; Choi, Y. W.; Jun, G. H.; Lee, D. J.; Kong, B. S.; Paik, K.-W.; Jeon, S. Enhanced Thermal

Conductivity of Epoxy−Graphene Composites by Using Non-Oxidized Graphene Flakes with Non-Covalent Functionalization. *Adv. Mater.* **2013**, *25*, 732−737.
(18) Huxtable, S. T.; Cahill, D. G.; Shenogin, S.; Xue, L.; Ozisik, R.; Barone, P.; Usrey, M.; Strano, M. S.; Siddons, G.; Shim, M.; Keblinski, P. Interfacial Heat Flow in Carbon Nanotube Suspensions. *Nat. Mater.* **2003**, *2*, 731−734.
(19) Zürcher, J.; Goicochea, J.; Matsumoto, K.; Michel, B.; Brunschwiler, T. In *Centrifugal Formulation of Percolating Thermal Underfills for Flip-chip Applications*, Proceedings of 7th International Conference on Integrated Power Electronics Systems, Nuremberg, Germany, Mar 6−8; IEEE: New York, 2012, pp 1−6.
(20) Ganguli, S.; Roy, A. K.; Anderson, D. P. Improved Thermal Conductivity for Chemically Functionalized Exfoliated Graphite Epoxy Composites. *Carbon* **2008**, *46*, 806−817.
(21) Brunschwiler, T.; Schlottig, G.; Ni, S.; Liu, Y.; Goicochea, J. V.; Zürcher, J.; Wolf, H. Formulation of Percolating Thermal Underfills using Hierarchical Self-assembly of Micro- and Nanoparticles by Centrifugal Forces and Capillary Bridging. *J. Microelectron. Electron. Packag.* **2012**, *9*, 149−159.
(22) Kralchevsky, P. A.; Denkov, N. D. Capillary Forces and Structuring in Layers of Colloid Particles. *Curr. Opin. Colloid Interface Sci.* **2001**, *6*, 383−401.
(23) Quintard, M.; Whitaker, S. In *Handbook of Porous Media;* Vafai, K., Hadim, H. A., Eds.; Marcel Dekker: New York, NY, 2000; Chapter 2, pp 56−57.
(24) Pakpour, M.; Habibi, M.; Møller, P.; Bonn, D. How to Construct the Perfect Sandcastle. *Sci. Rep.* **2012**, *2*, 549.
(25) Rabinovich, Y. I.; Esayanur, M. S.; Moudgil, B. M. Capillary Forces between Two Spheres with a Fixed Volume Liquid Bridge: Theory and Experiment. *Langmuir* **2005**, *21*, 10992−10997.
(26) Wang, X.; Ishii, Y.; Ruslinda, A. R.; Hasegawa, M.; Kawarada, H. Effective Surface Functionalization of Nanocrystalline Diamond Films by Direct Carboxylation for PDGF Detection via Aptasensor. *ACS Appl. Mater. Interfaces* **2012**, *4*, 3526−3534.
(27) Geisler, M.; Hugel, T. Aging of Hydrogenated and Oxidized Diamond. *Adv. Mater.* **2010**, *22*, 398−402.